




Article

Structural Characteristics and Cementitious Behavior of Magnesium Slag in Comparison with Granulated Blast Furnace Slag

Ping Lu ^{1,2,3,4}, Yueqi Zhao ^{1,2,3,4} , Na Zhang ^{1,2,3,4,*} , Yidi Wang ^{1,2,3,4}, Jiale Zhang ^{1,2,3,4}, Yihe Zhang ^{1,2,3,4} and Xiaoming Liu ^{5,*} 

¹ Engineering Research Center of Ministry of Education for Geological Carbon Storage and Low Carbon Utilization of Resources, China University of Geosciences, Beijing 100083, China

² Beijing Key Laboratory of Materials Utilization of Nonmetallic Minerals and Solid Wastes, China University of Geosciences, Beijing 100083, China

³ National Laboratory of Mineral Materials, China University of Geosciences, Beijing 100083, China

⁴ School of Materials Science and Technology, China University of Geosciences, Beijing 100083, China

⁵ School of Metallurgical and Ecological Engineering, University of Science and Technology Beijing, Beijing 100083, China

* Correspondence: nazhang@cugb.edu.cn (N.Z.); liuxm@ustb.edu.cn (X.L.)

Abstract: Magnesium slag is a type of industrial solid waste produced during the production of magnesium metal. In order to gain a deeper understanding of the structure of magnesium slag, the composition and microstructure of magnesium slag were investigated by using characterization methods such as X-ray fluorescence, particle size analysis, X-ray diffraction, Fourier transform infrared spectroscopy and scanning electron microscopy. In addition, the state of Si occurrence in magnesium slag was analyzed using a solid-state nuclear magnetic resonance technique in comparison with granulated blast furnace slag. An inductively coupled plasma-optical emission spectrometer and scanning electron microscope with energy dispersive X-ray spectroscopy were used to characterize their cementitious behavior. The results show that the chemical composition of magnesium slag mainly includes 54.71% CaO, 28.66% SiO₂ and 11.82% MgO, and the content of Al₂O₃ is much lower than that of granulated blast furnace slag. Compared to granulated blast furnace slag, magnesium slag has a larger relative bridging oxygen number and higher [SiO₄] polymerization degree. The cementitious activity of magnesium slag is lower compared to that of granulated blast furnace slag, but it can replace part of the cement to obtain higher compressive strength. Maximum compressive strength can be obtained when the amount of magnesium slag replacing cement is 20%, where the 28-day compressive strength can be up to 45.48 MPa. This work provides a relatively comprehensive analysis of the structural characteristics and cementitious behavior of magnesium slag, which is conducive to the promotion of magnesium slag utilization.

Keywords: magnesium slag; granulated blast furnace slag; structural characterization; nuclear magnetic resonance; cementitious activity



Citation: Lu, P.; Zhao, Y.; Zhang, N.; Wang, Y.; Zhang, J.; Zhang, Y.; Liu, X. Structural Characteristics and Cementitious Behavior of Magnesium Slag in Comparison with Granulated Blast Furnace Slag. *Materials* **2024**, *17*, 360. <https://doi.org/10.3390/ma17020360>

Academic Editor: Krzysztof Schabowicz

Received: 29 November 2023

Revised: 28 December 2023

Accepted: 5 January 2024

Published: 11 January 2024



Copyright: © 2024 by the authors. Licensee MDPI, Basel, Switzerland. This article is an open access article distributed under the terms and conditions of the Creative Commons Attribution (CC BY) license (<https://creativecommons.org/licenses/by/4.0/>).

1. Introduction

Magnesium slag is an industrial solid waste generated during the production of magnesium metal. In China, the smelting of magnesium metal via the Pijiang method is the main commercial process for magnesium production [1,2]. More than 6 tons of magnesium slag is produced when smelting 1 ton of magnesium metal on average, and it is accompanied by nearly 30 tons of CO₂ and various types of flue gas emissions [3], which seriously pollute the environment of the area where it is located [4]. At present, there is no complete treatment technology for magnesium slag to enable its industrial utilization, which leads to massive accumulation of magnesium slag in the open air [5]. This not only

takes up considerable land resources and damages the ecological environment, but also poses a threat to human health [6–9]. Like other industrial solid wastes, if magnesium slag can be effectively utilized, this will bring great ecological and economic benefits [10–14], promoting the early realization of China's goal of "carbon peak and carbon neutrality" according to the Paris Agreement.

Magnesium slag mainly contains CaO, SiO₂ and MgO. Due to its high MgO content, expansion behavior occurs during the hydration process [15–17], and for that reason, magnesium slag is not yet used on a large scale in the construction industry. Ji et al. [18] discussed the potential of magnesium slag as a mineral admixture and found that when 30% of magnesium slag was used as a replacement for Portland cement, this was beneficial to improve the late strength of concrete and reduce drying shrinkage. Xie et al. [19] used magnesium slag as an admixture for low-carbon cement, and the prepared samples met the GB 175-2007 [20] "General Portland Cement" standard, which could reduce the production cost by more than 10%. The synthesis of porous materials from magnesium slag can have a good adsorption effect on Pb²⁺ while the materials also have high compressive strength [21]. CO₂ solidified fiber cement boards prepared with magnesium slag as a binder had high flexural strength, carbonation rate and water absorption [22]. Using the "leaching-carbonization" method, magnesium slag can be turned into two value-added products: vaterite with a purity of more than 95% and supplementary cementitious materials [23]. Magnesium slag has limited activity in its normal state, making it difficult to be applied directly. Therefore, scholars use diverse approaches to stimulate its activity and improve applicability. Lei et al. [24] proposed CO₂ activated aerated concrete with a high admixture of magnesium slag, which is capable of achieving rapid carbonation to improve compressive strength, reduce environmental pollution caused by the accumulation of magnesium slag and also facilitate the large-scale utilization of CO₂. When cured in water at 60 °C [25], a magnesium slag product treated with CO₂ activation has good volume stability and does not display excessive expansion. The effect of volumetric instability can be eliminated after carbonation for 2 h. At the same time, carbonation treatment can quickly obtain higher compressive strength, reaching 90 MPa at 24 h [26]. The incorporation of magnesium slag can improve the soil environment by granularizing the soil and providing higher cementitious activity [27–29], and also has a remediation effect on Cd- and As-contaminated paddy soils [30]. Jia et al. [31] investigated the desulfurization characteristics of magnesium slag and achieved a calcium conversion of 30.3% for samples treated with continuous hydration under optimum process parameters. In addition, magnesium slag can be used as a raw material for the preparation of phosphate adsorbents [32], with a maximum adsorption capacity of up to 50.14 mg/g. The Fe₂O₃ content in magnesium slag has a large effect on the phosphorus removal rate, which can also be enhanced after acid treatment [33]. Whilst the desulfurization performance of the original magnesium slag is poor, a calcium conversion rate of up to 73.7% can be reached after mixing with additives or modification [34]. Magnesium slag, like other solid wastes, can also be used for mine filling [5,35,36] or road base material [37–42]. Numerous studies have conducted extensive research into other industrial solid wastes, such as granulated blast furnace slag [43–45], steel slag [46], red mud [47] and so on [48–50], which provide guidance for the utilization of the corresponding tailings and slag. However, there are fewer corresponding studies on the structure and cementitious properties of magnesium slag, which is one of the reasons for its current low utilization. Accordingly, there is an urgent need to study the structural characteristics of magnesium slag and propose avenues to utilize it in an efficient and resourceful way.

This work aimed to study the structural characteristics and cementitious activity of magnesium slag in comparison with those of granulated blast furnace slag using X-ray diffraction (XRD), Fourier transform infrared spectroscopy (FTIR) and ²⁹Si solid-state nuclear magnetic resonance (NMR). The cementitious activity of magnesium slag and granulated blast furnace slag under alkaline conditions were assessed through the dissolution of Si, Al and Mg elements in alkaline solutions. Hydration behavior of magnesium slag

and granulated blast furnace slag was investigated using scanning electron microscopy and energy dispersive X-ray spectrometry (SEM-EDS), and the possibility of their replacement for cement was also discussed. The results of this study may contribute to a deeper understanding of the relationship between the microstructure and cementitious activity of magnesium slag, which will provide basic knowledge for further comprehensive utilization of magnesium slag. Additionally, this work compares the cementitious activity of magnesium slag with that of granulated blast furnace slag for the first time, which is of great reference value to the field of magnesium slag utilization.

2. Experimental Program

Details of the raw materials and related test parameters used in this work are shown below.

2.1. Raw Materials

The magnesium slag used in the experiment was provided by Dongfeng Magnesium Metal Co., Ltd. of Yulin City, Shaanxi Province, China. The 42.5 Portland cement and granulated blast furnace slag were supplied by Henan Yuanheng Environmental Protection Engineering Co., Ltd, Henan, China. The NaOH was sourced from Yili Fine Chemicals Co., Ltd., Beijing, China. The chemical compositions of magnesium slag (MS) and granulated blast furnace slag (GBFS) as determined via X-ray fluorescence spectrometry (XRF) are shown in Table 1.

Table 1. Chemical composition of raw materials.

Chemical Composition (wt%)	CaO	SiO ₂	Al ₂ O ₃	MgO	Fe ₂ O ₃	SO ₃	TiO ₂	Others
MS	54.71	28.66	0.85	11.82	2.87	0.07	0.06	0.96
GBFS	42.76	27.85	15.61	7.78	0.36	2.64	1.20	2.16
Cement	71.52	15.08	3.59	1.81	3.44	3.03	0.43	1.10

2.2. Characterization Methods

2.2.1. Particle Size

The bulk magnesium slag was first crushed by a jaw crusher and then added into a ball mill and ground at 600 rpm for 2 h to obtain magnesium slag powder. The particle size of magnesium slag powder and granulated blast furnace slag powder was tested using a laser particle size analyzer (Bettersize2000, Dandong Baxter Instrument Co., Ltd., Dandong, China), where sodium hexametaphosphate was used as a dispersant.

2.2.2. X-ray Diffraction

The mineralogical components of magnesium slag were analyzed via X-ray powder diffraction (XRD) (Bruker D8 Advance Instrument, Bruker Corporation, Karlsruhe, Germany) using Cu K α radiation ($\lambda = 1.54056 \text{ \AA}$) at 40 kV and 40 mA. The scanning range was $5^\circ \sim 90^\circ$ and the scanning speed was $5^\circ/\text{min}$.

2.2.3. Nuclear Magnetic Resonance

In order to obtain more accurate solid-state NMR test results, small amounts of magnetic material were removed from the magnesium slag and granulated blast furnace slag, and then they were tested using an NMR spectrometer (AVANCE III 600M, Bruker Corporation, Karlsruhe, Germany).

2.2.4. Compressive Strength

Initially, 100 g of slag powder was added to a paste mixer, stirred, vibrated and finally poured into molds. After demolding, $20 \times 20 \times 20$ mm paste specimens were obtained, and the compressive strength of specimens at different curing ages was tested using a

microcomputer-controlled electro-hydraulic servo universal testing machine (WAW-2000E, Jinan Kohui Testing Equipment Co., Ltd., Jinan, China).

2.2.5. Inductively Coupled Plasma-Optical Emission Spectrometer

The active element contents (Si, Al, Mg) of magnesium slag and granulated blast furnace slag dissolved in an alkaline environment, were determined using an inductively coupled plasma instrument (ICAP-7000, Thermo Fisher, Waltham, MA, USA). The specific operations were as follows: 1 g of slag powder was added to 50 mL of 1 mol/L NaOH solution, sealed and left to stand for 72 h at room temperature, after which the upper layer of clear liquid was taken following centrifugation for ICP testing.

2.2.6. Scanning Electron Microscope

The above centrifuged liquid was poured out, and anhydrous ethanol was added to terminate the hydration of the solids for 48 h, after which the solids were put into a vacuum drying oven to dry sufficiently for 24 h. The microscopic morphology of the samples was observed and analyzed using an SU 8020 field emission scanning electron microscope (SU 8020, Hitachi Ltd., Tokyo, Japan).

3. Results

3.1. Mineralogical Composition of Magnesium Slag

Figure 1 demonstrates the XRD pattern of magnesium slag. The results show that the main phases of magnesium slag are quartz (SiO_2), larnite ($\beta\text{-Ca}_2\text{SiO}_4$), calcio-olivine ($\gamma\text{-Ca}_2\text{SiO}_4$), calcium silicate (Ca_3SiO_5) and periclase (MgO). Table 2 shows the results of the quantitative XRD analysis of magnesium slag. It was found that magnesium slag contains 58.4 wt% larnite ($\beta\text{-Ca}_2\text{SiO}_4$), 27.1 wt% quartz (SiO_2) and small amounts of Ca_3SiO_5 , MgO and $\gamma\text{-Ca}_2\text{SiO}_4$. Compared with $\gamma\text{-Ca}_2\text{SiO}_4$, $\beta\text{-Ca}_2\text{SiO}_4$ has higher cementitious activity, and the high content of $\beta\text{-Ca}_2\text{SiO}_4$ in magnesium slag provides great potential for its application in cementitious materials.

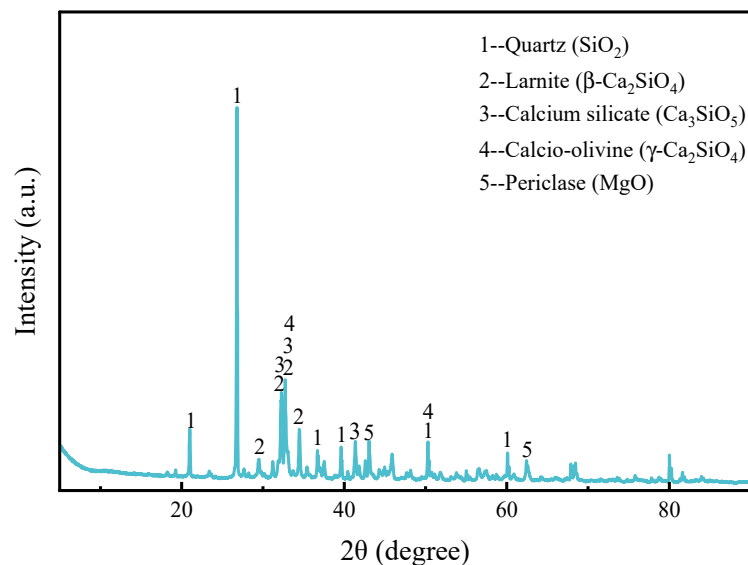


Figure 1. XRD pattern of magnesium slag.

Table 2. Quantitative XRD analysis of magnesium slag.

Mineralogical Composition (wt%)	SiO_2	$\beta\text{-Ca}_2\text{SiO}_4$	$\gamma\text{-Ca}_2\text{SiO}_4$	Ca_3SiO_5	MgO
MS	27.1	58.4	2.6	7.1	4.8

Figure 2 shows the FTIR results of magnesium slag. The main vibrational bands of magnesium slag are at 519 cm^{-1} , 846 cm^{-1} , 895 cm^{-1} , 995 cm^{-1} , 1426 cm^{-1} and 1633 cm^{-1} . Among them, the Mg-O vibrational band is at 519 cm^{-1} , and the stretching vibrational band of Si-O in SiO_2 is at 995 cm^{-1} . The bands at 846 cm^{-1} , 895 cm^{-1} and 1426 cm^{-1} are the vibrational bands of silica–aluminum matter, and the absorption band located at 1633 cm^{-1} is related to the bending vibration of the H-O-H group of bound water.

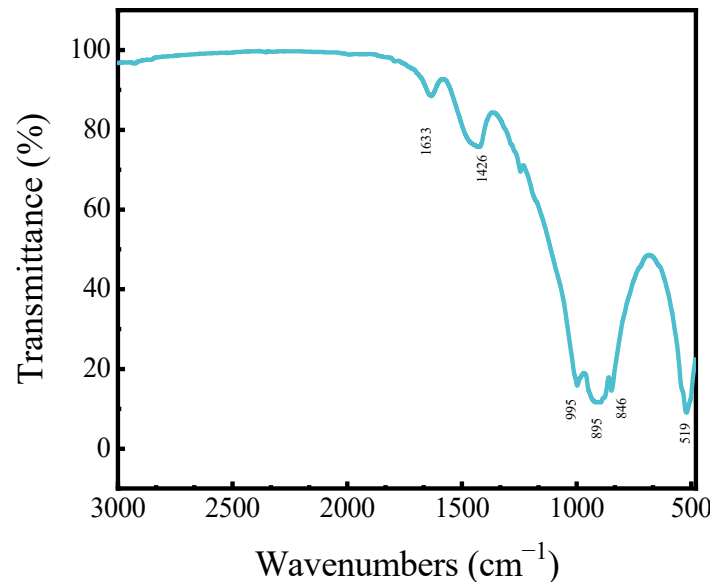


Figure 2. Infrared spectra of magnesium slag.

3.2. $[\text{SiO}_4]$ Polymerization Degree of Magnesium Slag and Granulated Blast Furnace Slag

In order to clarify the relationship between the cementitious activity and structure of magnesium slag, solid-state ^{29}Si NMR analysis was performed to further study the $[\text{SiO}_4]$ polymerization degree of magnesium slag in comparison with granulated blast furnace slag [51]. Figure 3 shows the NMR spectra of magnesium slag and granulated blast furnace slag. As can be seen from Figure 3, there are two main resonance peaks in the magnesium slag. According to the relationship between their chemical shifts and structures, the resonance peak at about -70 ppm belongs to SiQ^0 , and the resonance peak at about -115 ppm belongs to SiQ^4 . The resonance peak of granulated blast furnace slag only at about -73 ppm belongs to SiQ^0 . This suggests that SiO_4 tetrahedra in magnesium slag exist as nesosilicates and framework silicate [52], which is consistent with the quantitative analysis results of XRD.

Figure 4 shows the split peak fitting results of the two main peaks in the ^{29}Si NMR spectrum of magnesium slag. Five independent resonance peaks were obtained by splitting the two main peaks of magnesium slag using PeakFit software (v4.04), and their areas were calculated separately. The resonance peaks at -66.89 ppm , -70.46 ppm and -73.40 ppm belong to SiQ^0 , and the resonance peaks at -112.25 ppm and -115.77 ppm belong to SiQ^4 . The results are shown in Table 3. According to the relative bridging oxygen number (RBO) calculation formula [52],

$$RBO = \frac{1}{4} \cdot \frac{\sum n \cdot Q^n}{\sum Q^n} = \frac{1}{4} \left(1 \times \frac{Q^1}{\sum Q^n} + 2 \times \frac{Q^2}{\sum Q^n} + 3 \times \frac{Q^3}{\sum Q^n} + 4 \times \frac{Q^4}{\sum Q^n} \right)$$

$$RBO(MS) = \frac{1}{4} \cdot \frac{0 \cdot Q^0 + 4 \cdot Q^4}{Q^0 + Q^4}$$

it can be calculated that the RBO number of magnesium slag is 0.52. Generally speaking, the greater the relative bridging oxygen number, the higher the $[\text{SiO}_4]$ polymerization degree and the lower the cementitious activity of the slag. Granulated blast furnace slag is mainly composed of a SiQ^0 unit with an RBO number of 0. Its $[\text{SiO}_4]$ polymerization

degree is lower than that of magnesium slag, so the cementitious activity of granulated blast furnace slag is higher than that of magnesium slag.

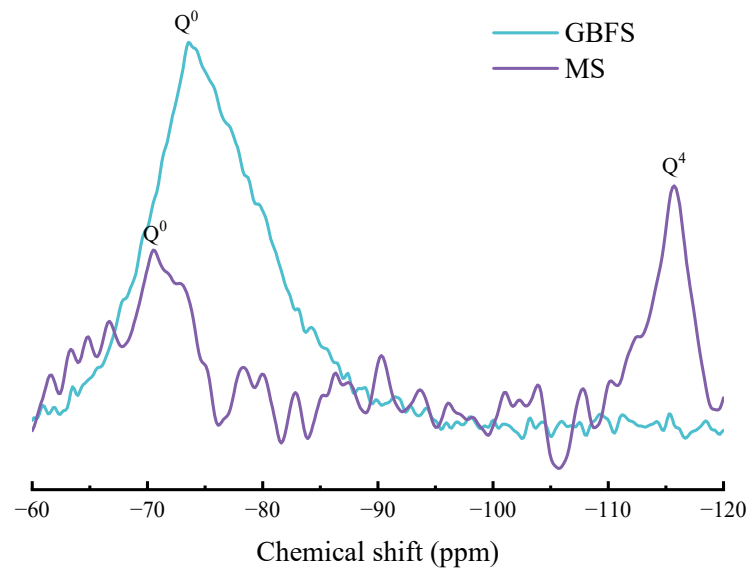


Figure 3. ²⁹Si NMR spectra of magnesium slag and granulated blast furnace slag.

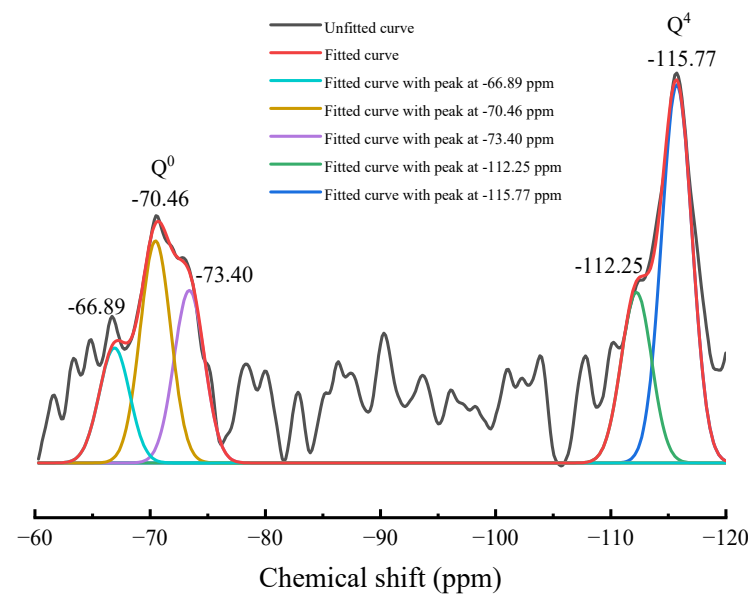


Figure 4. Peak-fitting results of ²⁹Si NMR spectrum of magnesium slag.

Table 3. RBO calculation of magnesium slag.

Structure Units	Q ⁰	Q ⁰	Q ⁰	Q ⁴	Q ⁴
Chemical shift (ppm)	-66.89	-70.46	-73.40	-112.25	-115.77
Relative area	30.42	58.74	45.64	45.14	100
Relative content (%)	10.87	20.98	16.30	16.13	35.72

3.3. Alkali-Activated Behavior of Magnesium Slag and Granulated Blast Furnace Slag

The ability of slag powder to release reactive ions SiO_4^{4-} and AlO_2^- in alkaline solution can reflect its cementitious activity [53]. In order to investigate the amount of active ions produced by magnesium slag in alkaline solution, magnesium slag powder and granulated blast furnace slag were activated with NaOH solution to assess any difference in cementitious activity.

The dissolution results shown in Figure 5 demonstrate both magnesium slag and granulated blast furnace slag, in which no magnesium element with cementitious activity is dissolved. Magnesium slag can dissolve a certain amount of Si and Al, while granulated blast furnace slag dissolves more. Combined with Table 1, we can surmise that the SiO_2 content in magnesium slag is slightly higher than that in granulated blast furnace slag. However, the dissolved amount of Si in granulated blast furnace slag is about six times that of magnesium slag. As the content of Al_2O_3 in granulated blast furnace slag is about twenty times higher than that in magnesium slag, the dissolved amount of Al in granulated blast furnace slag is much higher than that of magnesium slag, reaching nearly 30 times more. Figure 6 shows the particle size distribution of magnesium slag and granulated blast furnace slag. It can be found that the particle size of magnesium slag powder is smaller than that of granulated blast furnace slag. In general, a smaller particle size makes it easier for a pozzolanic reaction to occur completely. However, the results of alkali dissolution are the opposite of this. These results indicate that magnesium slag powder has a certain cementitious activity, but this is much lower than that of granulated blast furnace slag.

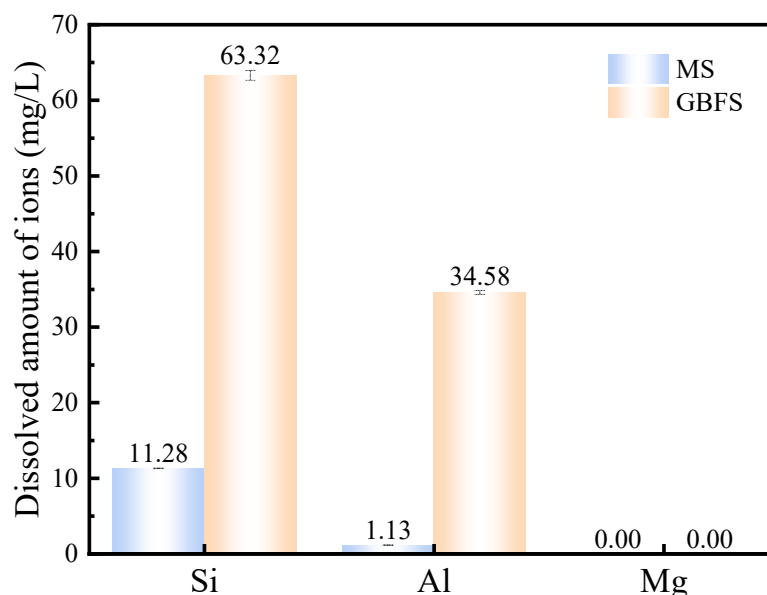


Figure 5. Dissolution content of Si, Al and Mg ions in 1 mol/L NaOH solution for magnesium slag and granulated blast furnace slag.

3.4. Microstructure of Magnesium Slag and Granulated Blast Furnace Slag

Figure 7 shows SEM images of granulated blast furnace slag and magnesium slag samples and the corresponding samples after alkali dissolution. It can be observed that both the granulated blast furnace slag and magnesium slag were in the form of flakes with a relatively smooth surface. After alkali dissolution, the morphology of slags changed from the original flake to an agglomerate, and C-A-S-H gel formed on the surface. The slags before and after alkali dissolution were analyzed using EDS, and the results are shown in Figure 8 and Table 4. The amount of each element in the granulated blast furnace slag and magnesium slag decreased significantly after alkali dissolution, except for O, which indicates that these other elements, after alkali dissolution, are involved in the formation of C-A-S-H gel. It is noted that the consumption of each element of granulated blast furnace slag is much higher than that of magnesium slag, which may indicate that granulated blast furnace slag has higher cementitious activity than magnesium slag. This is consistent with the above ICP analysis results.

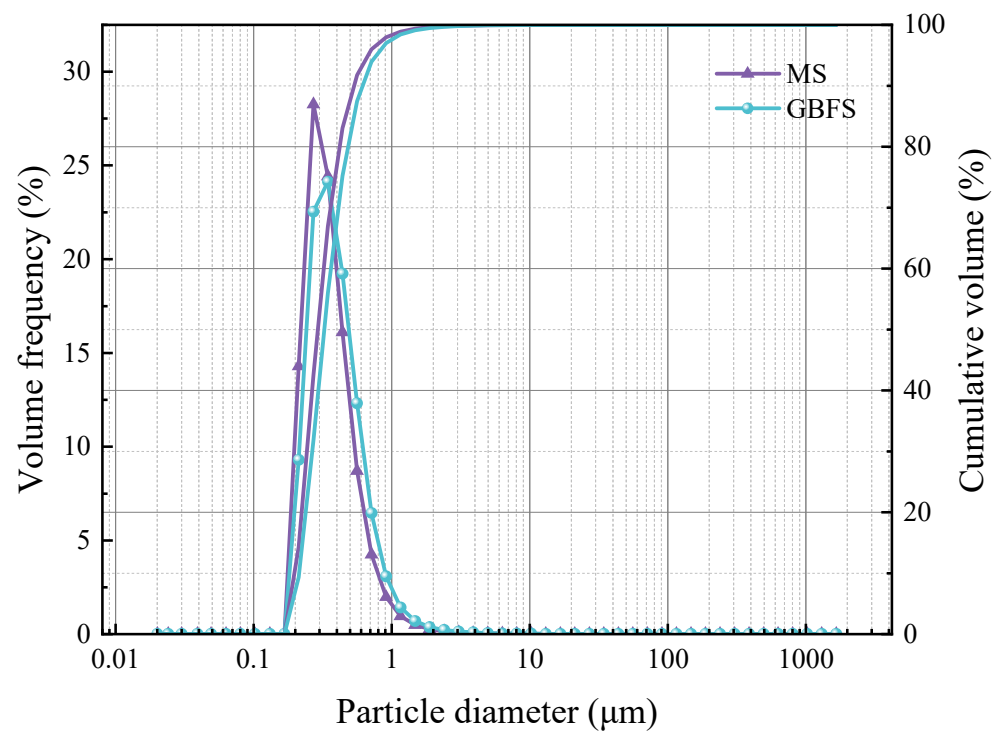


Figure 6. Particle size distribution of magnesium slag and granulated blast furnace slag.

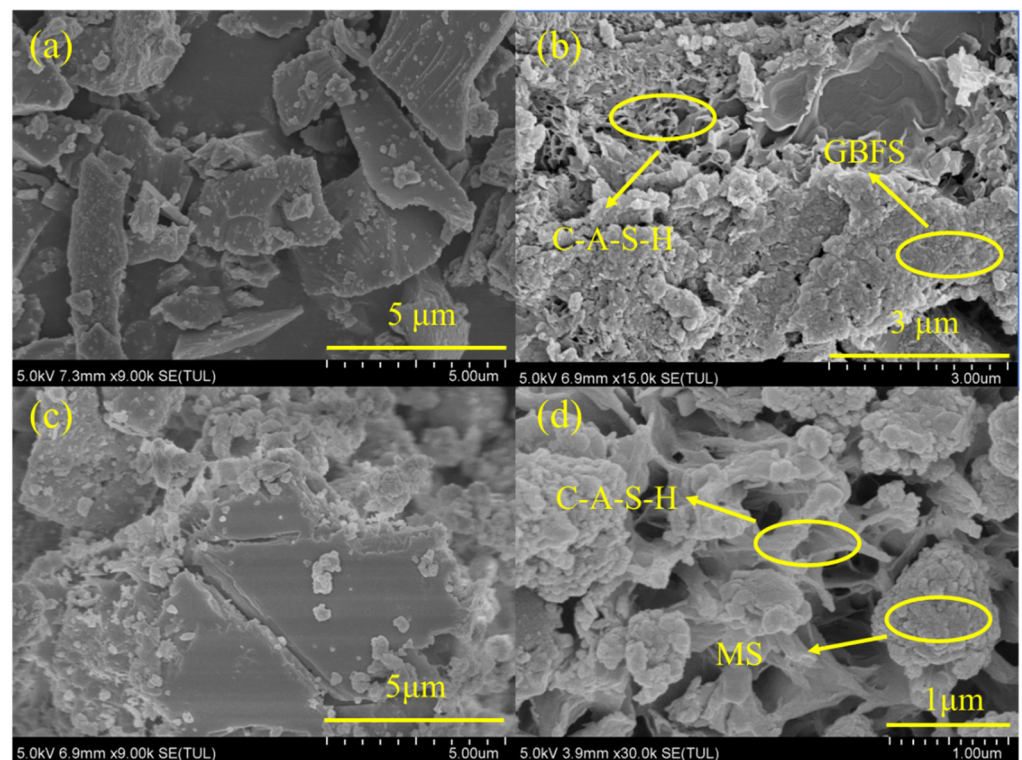


Figure 7. SEM images of GBFS (a) and GBFS after alkali dissolution (b); SEM images of MS (c) and MS after alkali dissolution (d).

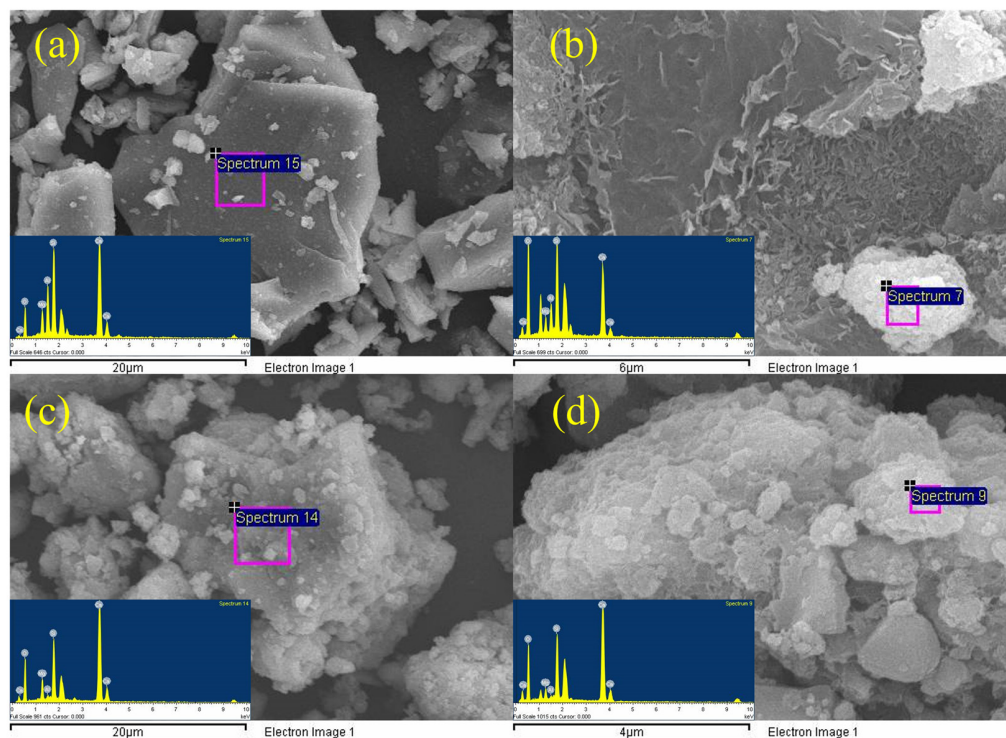


Figure 8. SEM-EDS analysis of GBFS (a) and GBFS after alkali dissolution (b); SEM-EDS analysis of MS (c) and MS after alkali dissolution (d).

Table 4. SEM-EDS analysis results.

Sample	O (Atomic%)	Mg (Atomic%)	Al (Atomic%)	Si (Atomic%)	Ca (Atomic%)
a	57.60	4.69	7.26	13.90	16.55
b	77.85	2.17	2.90	9.51	7.57
c	71.64	3.91	0.44	8.39	15.63
d	76.48	1.87	0.22	8.04	13.39

3.5. Magnesium Slag and Granulated Blast Furnace Slag as Replacements for Cement

In order to further confirm cementitious activity, magnesium slag and granulated blast furnace slag were used to replace a part of Portland cement in a paste experiment to compare the feasibility of their uses as a mineral admixture. Figure 9 shows samples of 20 × 20 × 20 mm paste prepared with reference to the literature [54] and standard [55], which were used for compressive strength testing after curing for the corresponding ages. Figures 10 and 11 show the compressive strength of blended cement after partial replacement with magnesium slag and granulated blast furnace slag, respectively. It is beneficial to increase the compressive strength when a small amount of magnesium slag is used to replace the cement. However, the compressive strength of the samples drops below that of pure cement when more than 20% of cement is replaced by magnesium slag. The main reason is that magnesium slag has limited activity in this condition without alkali activation. When the amount of magnesium slag in the system is less than 20%, Ca(OH)₂ produced during the hydration process of cement can play a significant role in activating the magnesium slag, so that the magnesium slag can better participate in the hydration process [56]. As a result, magnesium slag can be used to replace part of the cement within a 20% dosage whilst the compressive strength can also be improved. However, when the amount of magnesium slag continues to increase, the amount of Ca(OH)₂ produced through cement hydration decreases, resulting in a decrease in alkali concentration in the hydrated system, and thus the activity of magnesium slag is not well-activated. Therefore, the

compressive strength declines with increasing amounts of magnesium slag exceeding 20% addition. As shown in Figure 10, a similar phenomenon is observed when using granulated blast furnace slag to replace part of the cement. When the amount of replacement exceeds 20%, the 28-day compressive strength of the granulated blast furnace slag–cement samples gradually decreases with an increase in granulated blast furnace slag dosage. However, the compressive strength is still higher than that of the pure cement when a 50% dosage of granulated blast furnace slag is used for the replacement of cement, strongly indicating that granulated blast furnace slag is a valuable mineral admixture in cement and concrete. Moreover, due to the higher alkali activity of granulated blast furnace slag than that of the magnesium slag, it is found that the compressive strength of the granulated blast furnace slag–cement system is higher than that of the magnesium slag–cement group at the same replacement amount. These results suggest that although the cementitious activity of magnesium slag is lower than that of granulated blast furnace slag, magnesium slag can still be used as a mineral admixture for replacing a 20% amount of cement in blended cementitious materials.



Figure 9. Samples for compressive strength test.

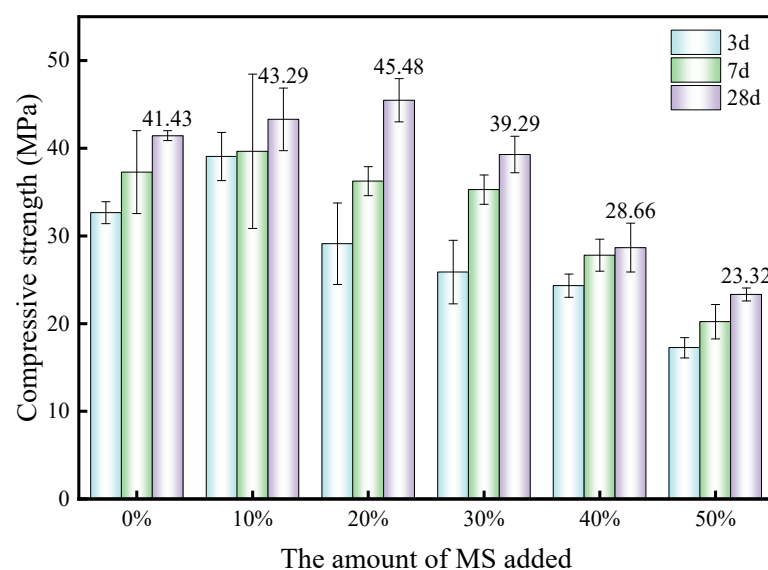


Figure 10. Compressive strengths of samples with different replacement amounts of magnesium slag.

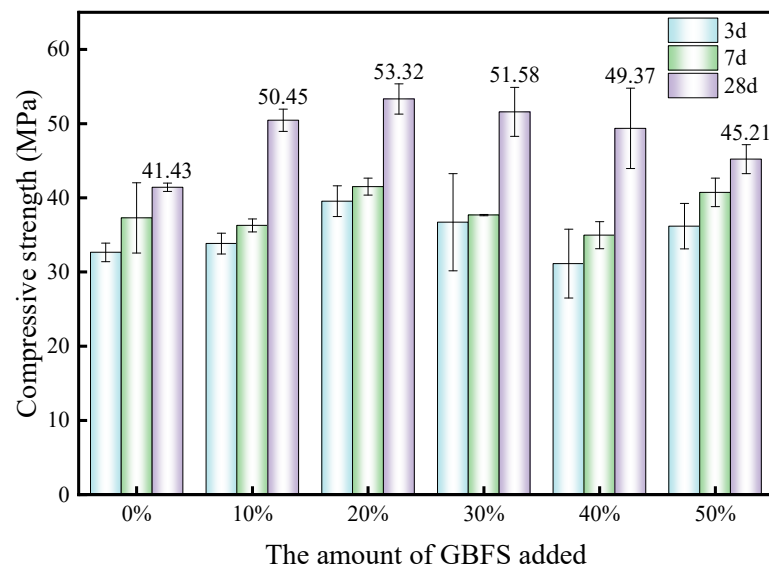


Figure 11. Compressive strengths of samples with different replacement amounts of granulated blast furnace slag.

Various methods exist to assess the cementitious activity of solid waste, such as conductivity tests, compressive strength tests, lime absorption methods and alkali dissolution methods [57–60]. Scholars have used these methods to scientifically evaluate the cementitious activity of granulated blast furnace slag [43], steel slag [46], red mud [47] and other tailings [61], but the link between the results has not been well-identified. This work investigated the structural properties and cementitious behavior of magnesium slag and granulated blast furnace slag by using NMR, compressive strength tests and alkali dissolution methods. A difference in activity between magnesium slag and granulated blast furnace slag was demonstrated in the results. These provide a reference for magnesium slag utilization as well as assessment of the cementitious activity of other tailings.

4. Conclusions

This work principally investigated the structural characteristics of magnesium slag and studied its cementitious properties in comparison with granulated blast furnace slag. The main conclusions drawn are as follows:

- (1) The chemical composition of magnesium slag is mainly CaO, SiO₂, Al₂O₃, MgO and Fe₂O₃. Its main components are similar to those of granulated blast furnace slag, but it contains more MgO and less Al₂O₃ than granulated blast furnace slag. The main mineral compositions of magnesium slag are 27.1% quartz, 58.4% larnite, 7.1% calcium silicate, 4.8% periclase and 2.6% calcio-olivine.
- (2) The Si in magnesium slag is mainly in the form of Q⁰ and Q⁴ units, which have a large relative bridging oxygen number and high [SiO₄] polymerization degree, resulting in relatively poor cementitious activity. The Si in granulated blast furnace slag is mainly in the form of Q⁰ units, and the relative bridging oxygen number is close to 0. Compared with magnesium slag, the degree of [SiO₄] polymerization is lower and the cementitious activity is higher for granulated blast furnace slag. After alkali excitation, the cementitious activity of magnesium slag can be reflected, and through this approach, we found that its cementitious activity is significantly lower than that of granulated blast furnace slag.
- (3) Both magnesium slag and granulated blast furnace slag can be used as mineral admixtures to replace part of cement. Higher compressive strength can be obtained after replacing cement with a small amount of magnesium slag, and the optimum replacement amount is 20%. With further increase of the replacement amount, the

compressive strength decreases, and when it exceeds 30%, the compressive strength of magnesium slag–cement samples is lower than that of pure cement.

- (4) Magnesium slag has the potential to be utilized as a mineral admixture for cement, but attention should be paid to the amount of magnesium slag added, activity excitation and the expansion of magnesium hydrate products during its application in cement and concrete production. Elimination of the expansion effect caused by f-MgO in magnesium slag is an important topic for our future work.

Author Contributions: Conceptualization, Y.Z. (Yihe Zhang); data curation, P.L., N.Z., Y.W. and J.Z.; formal analysis, P.L. and Y.Z. (Yueqi Zhao); investigation, P.L., Y.Z. (Yueqi Zhao), Y.W. and J.Z.; resources, Y.Z. (Yihe Zhang) and X.L.; supervision, N.Z. and X.L.; validation, N.Z. and X.L.; writing—original draft, P.L.; writing—review and editing, N.Z. and X.L. All authors have read and agreed to the published version of the manuscript.

Funding: This research was funded by the National Natural Science Foundation of China (no. 52174388).

Institutional Review Board Statement: Not applicable.

Informed Consent Statement: Not applicable.

Data Availability Statement: Data are contained within the article.

Conflicts of Interest: The authors declare no conflicts of interest.

References

1. Abedini Najafabadi, H.; Ozalp, N.; Epstein, M.; Davis, R. Solar Carbothermic Reduction of Dolomite: Direct Method for Production of Magnesium and Calcium. *Ind. Eng. Chem. Res.* **2020**, *59*, 14717–14728. [[CrossRef](#)]
2. Telgerafchi, A.E.; Rutherford, M.; Espinosa, G.; McArthur, D.; Mase, N.; Perrin, B.; Tang, Z.; Powell, A.C. Magnesium Production by Molten Salt Electrolysis with Liquid Tin Cathode and Multiple Effect Distillation. *Front. Chem.* **2023**, *11*, 1192202. [[CrossRef](#)] [[PubMed](#)]
3. Tian, Y.; Wang, L.; Yang, B.; Dai, Y.; Xu, B.; Wang, F.; Xiong, N. Comparative Evaluation of Energy and Resource Consumption for Vacuum Carbothermic Reduction and Pidgeon Process Used in Magnesium Production. *J. Magnes. Alloys* **2022**, *10*, 697–706. [[CrossRef](#)]
4. Djokic, J.; Minic, D.; Kamberovic, Z.; Petkovic, D. Impact Analysis of Airborne Pollution Due to Magnesium Slag Deposit and Climatic Changes Condition. *Ecol. Chem. Eng. S* **2012**, *19*, 439–450. [[CrossRef](#)]
5. Ruan, S.; Liu, L.; Zhu, M.; Shao, C.; Xie, L. Development and Field Application of a Modified Magnesium Slag-Based Mine Filling Cementitious Material. *J. Clean. Prod.* **2023**, *419*, 138269. [[CrossRef](#)]
6. Webber, M.E.; Glazer, Y.R. Solid Waste, a Lever for Decarbonization. *Science* **2023**, *382*, 762–763. [[CrossRef](#)]
7. Mishra, R.; Singh, E.; Kumar, A.; Ghosh, A.; Lo, S.-L.; Kumar, S. Co-Gasification of Solid Waste and Its Impact on Final Product Yields. *J. Clean. Prod.* **2022**, *374*, 133989. [[CrossRef](#)]
8. Doorga, J.R.S.; Rughooputh, S.D.D.V.; Chung, S.Y.; McGivern, A. A Geospatial Approach for Addressing Long-Term Solid Waste Management Issues: Extracting Value from Waste. *J. Clean. Prod.* **2022**, *334*, 130282. [[CrossRef](#)]
9. Khan, H.; Baig, A.; Faisal, M.; Khan, A.; Gul, K.; Ali, N.; Ali, N.; Bilal, M. Exploration of Solid Waste Materials for Sustainable Manufacturing of Cementitious Composites. *Environ. Sci. Pollut. Res.* **2022**, *29*, 86606–86615. [[CrossRef](#)]
10. Nedunuri, A.S.S.S.; Muhammad, S. Fundamental Understanding of the Setting Behaviour of the Alkali Activated Binders Based on Ground Granulated Blast Furnace Slag and Fly Ash. *Constr. Build. Mater.* **2021**, *291*, 123243. [[CrossRef](#)]
11. Zakira, U.; Zheng, K.; Xie, N.; Birgisson, B. Development of High-Strength Geopolymers from Red Mud and Blast Furnace Slag. *J. Clean. Prod.* **2023**, *383*, 135439. [[CrossRef](#)]
12. Baalamurugan, J.; Kumar, V.G.; Padmapriya, R.; Raja, V.K.B. Recent Applications of Steel Slag in Construction Industry. *Environ. Dev. Sustain.* **2023**. [[CrossRef](#)]
13. Schatzmayr Welp Sá, T.; Oda, S.; Karla Castelo Branco Louback Machado Balthar, V.; Dias Toledo Filho, R. Use of Iron Ore Tailings and Sediments on Pavement Structure. *Constr. Build. Mater.* **2022**, *342*, 128072. [[CrossRef](#)]
14. Oprčkal, P.; Mladenovič, A.; Zupančič, N.; Ščančar, J.; Milačič, R.; Zalar Serjun, V. Remediation of Contaminated Soil by Red Mud and Paper Ash. *J. Clean. Prod.* **2020**, *256*, 120440. [[CrossRef](#)]
15. Nugmanova, A.; Shon, C.-S.; Kim, J.R.; Rossi, C.O. Characterizing Chronologically Aged Basic Oxygen Furnace Slags as Aggregates and Their Use in Asphalt Concrete Mix as Filler. *Appl. Sci.* **2023**, *13*, 10126. [[CrossRef](#)]
16. Imashuku, S.; Tsuneda, H.; Wagatsuma, K. Effects of Divalent-Cation Iron and Manganese Oxides on the Luminescence of Free Lime and Free Magnesia. *Spectrochim. Acta Part A Mol. Biomol. Spectrosc.* **2020**, *229*, 117952. [[CrossRef](#)]

17. Imashuku, S.; Wagatsuma, K. Scanning Electron Microscopy-Cathodoluminescence Imaging of Industrial Steelmaking Slag for Identifying and Determining the Free Magnesia Content. *Met. Mater Trans B* **2022**, *53*, 3459–3468. [[CrossRef](#)]
18. Ji, G.; Peng, X.; Wang, S.; Hu, C.; Ran, P.; Sun, K.; Zeng, L. Influence of Magnesium Slag as a Mineral Admixture on the Performance of Concrete. *Constr. Build. Mater.* **2021**, *295*, 123619. [[CrossRef](#)]
19. Xie, G.; Liu, L.; Suo, Y.; Zhu, M.; Yang, P.; Sun, W. High-Value Utilization of Modified Magnesium Slag Solid Waste and Its Application as a Low-Carbon Cement Admixture. *J. Environ. Manag.* **2024**, *349*, 119551. [[CrossRef](#)]
20. GB 175-2007; General Portland Cement. Chinese Standard Press: Beijing, China, 2007.
21. Lu, G.; Han, J.; Chen, Y.; Xue, H.; Qiu, R.; Zhou, X.; Ma, Z. Synthesis of Porous Materials Using Magnesium Slag and Their Adsorption Performance for Lead Ions in Aqueous Solution. *Materials* **2023**, *16*, 7083. [[CrossRef](#)]
22. Xie, D.; Zhang, Z.; Liu, Z.; Wang, F.; Hu, S.; Fu, J. Utilization of Magnesium Slag to Prepare CO₂ Solidified Fiber Cement Board. *Constr. Build. Mater.* **2024**, *411*, 134345. [[CrossRef](#)]
23. Lu, B.; Zhou, Y.; Jiang, L.; Liu, Z.; Hou, G. High-Purity Vaterite CaCO₃ Recovery through Wet Carbonation of Magnesium Slag and Leaching Residue Utilization in Cement. *Cem. Concr. Compos.* **2024**, *145*, 105353. [[CrossRef](#)]
24. Lei, M.; Deng, S.; Huang, K.; Liu, Z.; Wang, F.; Hu, S. Preparation and Characterization of a CO₂ Activated Aerated Concrete with Magnesium Slag as Carbonatable Binder. *Constr. Build. Mater.* **2022**, *353*, 129112. [[CrossRef](#)]
25. Mo, L.; Hao, Y.; Liu, Y.; Wang, F.; Deng, M. Preparation of Calcium Carbonate Binders via CO₂ Activation of Magnesium Slag. *Cem. Concr. Res.* **2019**, *121*, 81–90. [[CrossRef](#)]
26. Zhang, C.; Liu, S.; Tang, P.; Guan, X.; Shi, C. Enhancing the Hardening Properties and Microstructure of Magnesium Slag Blocks by Carbonation-Hydration Sequential Curing. *J. Build. Eng.* **2023**, *76*, 107414. [[CrossRef](#)]
27. Amini, O.; Ghasemi, M. Laboratory Study of the Effects of Using Magnesium Slag on the Geotechnical Properties of Cement Stabilized Soil. *Constr. Build. Mater.* **2019**, *223*, 409–420. [[CrossRef](#)]
28. Omid, A.; Mojtaba, G. Geotechnical Properties of Lime-Magnesium Slag Stabilized Clayey Sand: Experimental Study. *Arab. J. Sci. Eng.* **2022**, *47*, 13673–13685. [[CrossRef](#)]
29. Sipahutar, I.A.; Siregar, A.F.; Anggria, L. Husnain Magnesium and Silicon Fertilizer Application to Promote Rice Growth and Production. *IOP Conf. Ser. Earth Environ. Sci.* **2021**, *648*, 012064. [[CrossRef](#)]
30. Zhang, Y.; Tan, X.; Duan, G.; Cui, J.; Ren, M.; Cao, J.; Xu, C.; Yang, W.; Lin, A. Magnesium Slag for Remediation of Cadmium- and Arsenic-contaminated Paddy Soil: A Field Study. *Soil Use Manag.* **2022**, *38*, 1470–1480. [[CrossRef](#)]
31. Jia, L.; Fan, B.; Huo, R.; Li, B.; Yao, Y.; Han, F.; Qiao, X.; Jin, Y. Study on Quenching Hydration Reaction Kinetics and Desulfurization Characteristics of Magnesium Slag. *J. Clean. Prod.* **2018**, *190*, 12–23. [[CrossRef](#)]
32. Yang, B.; Han, F.; Li, Y.; Bai, Y.; Xie, Z.; Yang, J.; Liu, T. Phosphate Removal Mechanism of a Novel Magnesium Slag-Modified Coal Gasification Coarse Slag Adsorbent. *Environ. Sci. Pollut. Res.* **2023**, *30*, 60607–60617. [[CrossRef](#)] [[PubMed](#)]
33. Tang, X.; Li, R.; Wu, M.; Dong, L.; Wang, Z. Enhanced Phosphorus Removal Using Acid-Treated Magnesium Slag Particles. *Environ. Sci. Pollut. Res.* **2018**, *25*, 3860–3871. [[CrossRef](#)] [[PubMed](#)]
34. Fan, B.; Jia, L.; Li, B.; Huo, R.; Yao, Y.; Han, F.; Qiao, X.; Jin, Y. Study on Desulfurization Performances of Magnesium Slag with Different Hydration Modification. *J. Mater. Cycles. Waste Manag.* **2018**, *20*, 1771–1780. [[CrossRef](#)]
35. Akkaya, U.G.; Cinku, K.; Yilmaz, E. Characterization of Strength and Quality of Cemented Mine Backfill Made up of Lead-Zinc Processing Tailings. *Front. Mater.* **2021**, *8*, 740116. [[CrossRef](#)]
36. Sari, M.; Yilmaz, E.; Kasap, T.; Guner, N.U. Strength and Microstructure Evolution in Cemented Mine Backfill with Low and High pH Pyritic Tailings: Effect of Mineral Admixtures. *Constr. Build. Mater.* **2022**, *328*, 127109. [[CrossRef](#)]
37. Ramalakshmi, D.; Krishna, S.H. Study On Fly Ash as a Partial Replacement Material in Highway Embankment. *IOP Conf. Ser. Mater. Sci. Eng.* **2020**, *981*, 042094. [[CrossRef](#)]
38. Weiksnar, K.D.; Townsend, T.G. Enhancing the Chemical Performance of Phosphogypsum as a Road Base Material by Blending with Common Aggregates. *Resour. Conserv. Recycl.* **2024**, *200*, 107300. [[CrossRef](#)]
39. Al-Dossary, A.A.S.; Awed, A.M.; Gabr, A.R.; Fattah, M.Y.; El-Badawy, S.M. Performance Enhancement of Road Base Material Using Calcium Carbide Residue and Sulfonic Acid Dilution as a Geopolymer Stabilizer. *Constr. Build. Mater.* **2023**, *364*, 129959. [[CrossRef](#)]
40. Weiksnar, K.D.; Clavier, K.A.; Laux, S.J.; Townsend, T.G. Influence of Trace Chemical Constituents in Phosphogypsum for Road Base Applications: A Review. *Resour. Conserv. Recycl.* **2023**, *199*, 107237. [[CrossRef](#)]
41. Sofri, L.A.; Abdullah, M.M.A.B.; Sandu, A.V.; Imjai, T.; Vizureanu, P.; Hasan, M.R.M.; Almadani, M.; Aziz, I.H.A.; Rahman, F.A. Mechanical Performance of Fly Ash Based Geopolymer (FAG) as Road Base Stabilizer. *Materials* **2022**, *15*, 7242. [[CrossRef](#)]
42. Alzhanova, G.Z.; Aibuldinov, Y.K.; Iskakova, Z.B.; Khabidolda, S.M.; Abdiyussupov, G.G.; Omirzak, M.T.; Murali, G.; Vatin, N.I. Development of Environmentally Clean Construction Materials Using Industrial Waste. *Materials* **2022**, *15*, 5726. [[CrossRef](#)]
43. Schneider, J.; Cincotto, M.A.; Panepucci, H. ²⁹Si and ²⁷Al High-Resolution NMR Characterization of Calcium Silicate Hydrate Phases in Activated Blast-Furnace Slag Pastes. *Cem. Concr. Res.* **2001**, *31*, 993–1001. [[CrossRef](#)]
44. Puertas, F.; Fernández-Jiménez, A.; Blanco-Varela, M.T. Pore Solution in Alkali-Activated Slag Cement Pastes. Relation to the Composition and Structure of Calcium Silicate Hydrate. *Cem. Concr. Res.* **2004**, *34*, 139–148. [[CrossRef](#)]
45. Metlenkin, D.A.; Kiselev, N.V.; Platov, Y.T.; Khaidarov, B.B.; Khaidarov, T.B.; Kolesnikov, E.A.; Kuznetsov, D.V.; Gorokhovskiy, A.V.; Offor, P.O.; Burmistrov, I.N. Identification of the Elemental Composition of Granulated Blast Furnace Slag by FTIR-Spectroscopy and Chemometrics. *Processes* **2022**, *10*, 2166. [[CrossRef](#)]

46. Zhang, N.; Wu, L.; Liu, X.; Zhang, Y. Structural Characteristics and Cementitious Behavior of Basic Oxygen Furnace Slag Mud and Electric Arc Furnace Slag. *Constr. Build. Mater.* **2019**, *219*, 11–18. [[CrossRef](#)]
47. Liu, X.; Zhang, N.; Sun, H.; Zhang, J.; Li, L. Structural Investigation Relating to the Cementitious Activity of Bauxite Residue—Red Mud. *Cem. Concr. Res.* **2011**, *41*, 847–853. [[CrossRef](#)]
48. Richardson, I.G.; Brough, A.R.; Brydson, R.; Groves, G.W.; Dobson, C.M. Location of Aluminum in Substituted Calcium Silicate Hydrate (C-S-H) Gels as Determined by ²⁹Si and ²⁷Al NMR and EELS. *J. Am. Ceram. Soc.* **1993**, *76*, 2285–2288. [[CrossRef](#)]
49. Bediako, M.; Kevern, J.T.; Dodoo-Arhin, D. Co-Fired Ghanaian Clay-Palm Kernel Shells Pozzolan: Thermogravimetric, ²⁹Si and ²⁷Al MA NMR Characteristics. *Constr. Build. Mater.* **2017**, *153*, 430–435. [[CrossRef](#)]
50. Berenguer, R.; Lima, N.; Pinto, L.; Monteiro, E.; Povoas, Y.; Oliveira, R.; Lima, N.B.D. Cement-Based Materials: Pozzolanic Activities of Mineral Additions Are Compromised by the Presence of Reactive Oxides. *J. Build. Eng.* **2021**, *41*, 102358. [[CrossRef](#)]
51. Qoku, E.; Bier, T.A.; Schmidt, G.; Skibsted, J. Impact of Sulphate Source on the Hydration of Ternary Pastes of Portland Cement, Calcium Aluminate Cement and Calcium Sulphate. *Cem. Concr. Compos.* **2022**, *131*, 104502. [[CrossRef](#)]
52. Zhang, J.; Sun, H.; Sun, Y.; Zhang, N. Correlation between ²⁹Si Polymerization and Cementitious Activity of Coal Gangue. *J. Zhejiang Univ. Sci. A* **2009**, *10*, 1334–1340. [[CrossRef](#)]
53. Liu, X.; Liu, X.; Zhang, Z.; Wei, C.; Zeng, Q.; Li, Y.; Ma, S. Investigation of the Pozzolanic Activity Improvement of Yellow Phosphorus Slag with Thermal Activation. *Materials* **2023**, *16*, 6047. [[CrossRef](#)] [[PubMed](#)]
54. Meng, T.; Hong, Y.; Ying, K.; Wang, Z. Comparison of Technical Properties of Cement Pastes with Different Activated Recycled Powder from Construction and Demolition Waste. *Cem. Concr. Compos.* **2021**, *120*, 104065. [[CrossRef](#)]
55. GB/T50081; Standard for Test Method of Mechanical Properties on Ordinary Concrete. China National Standards: Beijing, China, 2002.
56. De Matos, P.R.; Andrade Neto, J.S.; Jansen, D.; De La Torre, A.G.; Kirchheim, A.P.; Campos, C.E.M. In-Situ Laboratory X-Ray Diffraction Applied to Assess Cement Hydration. *Cem. Concr. Res.* **2022**, *162*, 106988. [[CrossRef](#)]
57. Amar, M.; Benzerzour, M.; Abriak, N.-E.; Mamindy-Pajany, Y. Study of the Pozzolanic Activity of a Dredged Sediment from Dunkirk Harbour. *Powder Technol.* **2017**, *320*, 748–764. [[CrossRef](#)]
58. Martín, C.M.; Scarponi, N.B.; Villagrán, Y.A.; Manzanal, D.G.; Piqué, T.M. Pozzolanic Activity Quantification of Hollow Glass Microspheres. *Cem. Concr. Compos.* **2021**, *118*, 103981. [[CrossRef](#)]
59. Lorena Figueiredo Martins, M.; Roberto Ribeiro Soares Junior, P.; Henrique Da Silva, T.; De Souza Maciel, P.; Peixoto Pinheiro, I.; Cesar Da Silva Bezerra, A. Magnesium Industry Waste and Red Mud to Eco-Friendly Ternary Binder: Producing More Sustainable Cementitious Materials. *Constr. Build. Mater.* **2021**, *310*, 125172. [[CrossRef](#)]
60. Martins Torres, S.; Estolano de Lima, V.; de Azevedo Basto, P.; de Araújo Júnior, N.T.; de Melo Neto, A.A. Assessing the Pozzolanic Activity of Sugarcane Bagasse Ash Using X-Ray Diffraction. *Constr. Build. Mater.* **2020**, *264*, 120684. [[CrossRef](#)]
61. Rahman, S.A.; Dodd, A.; Khair, S.; Shaikh, F.U.A.; Sarker, P.K.; Hosan, A. Assessment of Lithium Slag as a Supplementary Cementitious Material: Pozzolanic Activity and Microstructure Development. *Cem. Concr. Compos.* **2023**, *143*, 105262. [[CrossRef](#)]

Disclaimer/Publisher's Note: The statements, opinions and data contained in all publications are solely those of the individual author(s) and contributor(s) and not of MDPI and/or the editor(s). MDPI and/or the editor(s) disclaim responsibility for any injury to people or property resulting from any ideas, methods, instructions or products referred to in the content.